THERMAL OPERATING WINDOW IN SELECTIVE LASER MELTING PROCESSES

Jerzy Kozak[1*] (iD)**, Tomasz Zakrzewski**[2] (iD)**, Marta Witt**[1] (iD) and **Martyna Dębowska-Wąsak**[1] (iD)
[1] Łukasiewicz Research Network – Institute of Aviation, Al. Krakowska 110/114, Warsaw 02-256, Poland
[2] General Electric, Al. Krakowska 110/114, Warsaw 02-256, Poland

Abstract
Selective laser melting (SLM) is one of the most effective methods of additive manufacturing (AM). It is used to manufacture products with very complex geometries using a wide range of materials. Practical process conditions are limited by the occurrence of undesirable melting instabilities that degrade the surface quality and lead to product defects. These disadvantages are related to the thermal limitations of the SLM process. The lower thermal limit is due to the need to completely melt the powder layer and partially remelt the underlying layer again to ensure proper bonding between the layers. Exceeding the upper thermal limit in the molten metal pool may cause extensive evaporation, boiling and ejection of molten metal droplets outside the melting area. The article presents an approach and methodology that enable the determination of thermal limits and the operating window of SLM/selective laser sintering (SLS) processes in a relatively simple way. The studies have been performed using various settings of SLM process parameters. The usefulness of the preliminary determination of thermal limitations and approximate prediction of operating window of SLM has been confirmed experimentally and by more accurate computer simulation.

Keywords: selective laser melting (SLM), thermal limitation, mathematical modeling, simulation
Type of the work: research article

NOMENCLATURE

A	Path cross-section area [m³]
C	Specific heat capacity [J/kg·K]
H	Powder bed thickness [μm]
h_t	Track height [m]
L	Specific latent heat [J/kg]
k_e	Thermal effective conductivity of powder [W/mK]
k_p	Track section profile coefficient [-]
P	Laser beam power [W]
P_d	Hatch spacing [μm]
r_e	Effective laser beam radius [μm]
T_m	Melting temperature [K]

* Corresponding Author: jerzy.kozak@ilot.lukasiewicz.gov.pl

T_b	Boiling temperature [K]
T_A	Lower temperature limit [K]
T_B	Upper temperature limit [K]
V	Laser scanning speed [mm/s]
W	Track width [m]
β	Porosity
ρ	Density [kg/m³]

1. INTRODUCTION

The laser additive manufacturing (AM) approach includes processes such as selective laser sintering (SLS) and selective laser melting (SLM) and is a repetitive, multilayer manufacturing process wherein a laser beam melts the material in a powder bed according to the slices of a corresponding three-dimensional (3D) computer-aided design (CAD) model. Stepwise production reduces complex 3D geometries into simpler 2D manufacturing steps, thus also reducing manufacturing restrictions. Because of the high geometric freedom that it provides, AM facilitates new impulses for the design of functional parts by having the potential to manufacture geometries that are impossible to manufacture using other processes. For these reasons, AM is now widely accepted as a new paradigm for the design and production of high-performance components for aerospace, medical, energy and automotive applications. Aerospace examples include complex fuel injector nozzles that previously required assembly of multiple parts and lightweight engineered structures that result in significant cost savings.

For example, the General Electric Company has successfully certified and implemented GE9X engine components such as T25 sensor housing, fuel nozzle tip and low-pressure turbine blades made using AM technologies (Fig. 1).
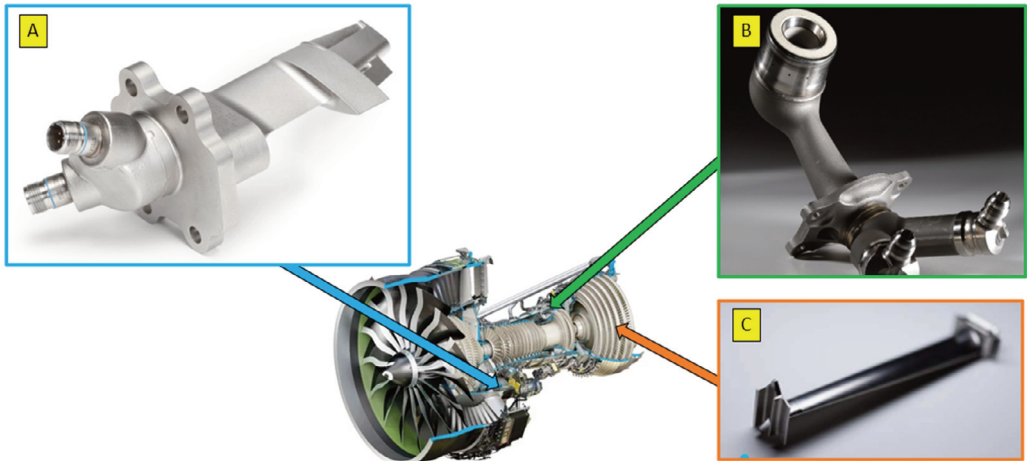

Figure 1. Additive manufactured GE9X engine components: (A) T25 sensor housing; (B) fuel nozzle tip; and (C) low-pressure turbine blades (adopted from reference [1]).

SLM is a three-step layer-based process using a powder bed: (1) a thin layer of metal powder is placed on a platform using a mechanical coating system; (2) a focused laser beam selectively melts the topmost

layer of the powder bed; and (3) after solidification, the platform is lowered by the layer thickness, and the cycle begins again. Complex parts can be built up, typically using thousands of layers.

In AM, processes comprise two stages, which include the following:

- the data preparation stage;
- the part manufacturing stage.

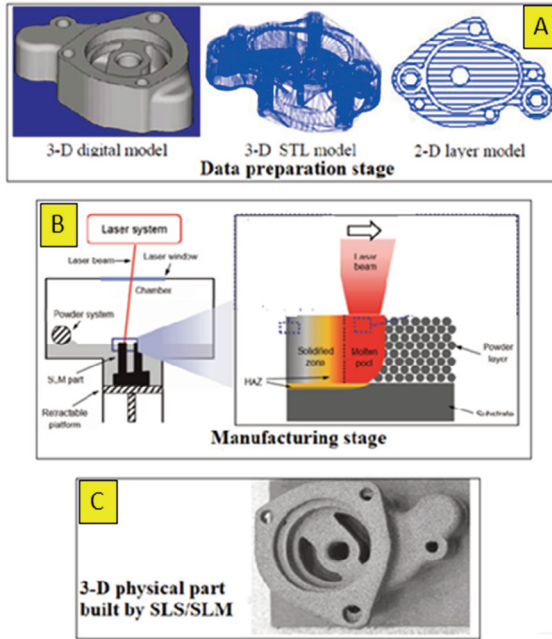The schematic diagram of these stages is shown in Fig. 2.

Figure 2. Scheme of the fabrication stages: A – data preparation, B – manufacturing stage, C – the physical part (figures adopted from reference [2]).

The schematic diagram of selective laser melting (SLM) and the various phenomena occurring during the process and that affect both the physical behaviour of the material and the final result of production are shown in Fig. 3.
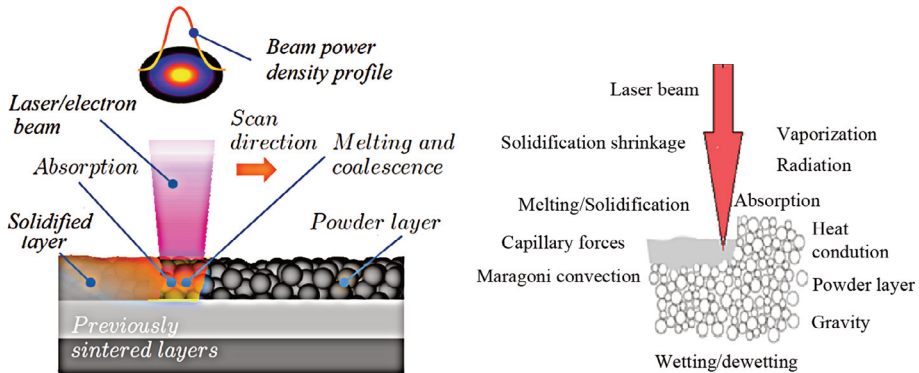

Figure 3. Schematic diagram of laser sintering melting (SLM) showing the key phenomena occurring during the process.

Particularly, the most important physical phenomena are powder melting, molten metal pool formation, keyhole formation, thermal fluid dynamics, vapourisation, spattering of powder and liquid/molten material, Marangoni effect, capillary effect, gaseous diffusion, instability of the pool, occurrence of powder particles and powder particles partially molten, remelting, excess heating, reheating and cooling, solidification, microstructural phase transformation, bending and shrinkage [3–10].

All these multiple physical processes and effects are highly influenced by several dozen process parameters, particularly laser power (P), laser spot size (d), scanning speed (V), path distance (P_d), layer thickness (h), energy density (E_d) and scanning strategy.

Improper parameters may lead to severe part-quality issues, such as defects in the manufactured part's structure.

Moreover, the manufacturer's recommended processing parameters often become obsolete with the introduction of new materials, technology upgrades and new SLM machines. Preparatory trial-and-error experiments are time-consuming and laborious. Therefore, fast screening of the proper process parameters is highly desirable for the SLM process, in pursuance of desired part quality, shortened design cycle and reduced production cost.

In the selection of SLM/SLS conditions, it is important to determine the range of operating parameters settings, called as the *manufacturing process parameters window* or *operating window*, which will ensure process stability and consequently avoid defects in the manufactured products [10, 18, 21].

The operating window of SLM processes is most often presented in the form of a set of points on the plane of parameters, such as plane {scan speed V, laser beam power P}.

The instability of the process means undesirable phenomena occurring during melting, evaporation and solidification, which lead to splashing of the material in a liquid state, balling effect, increase in porosity and poor interlayer cohesion, cracks and other defects.

In most of the works conducted to determine the process parameter window, experiments were carried out with a large number of samples. Based on the results of porosity or specific density measurements of the samples, a window of optimal parameters was determined. Based on statistical models, the relationship between the porosity or specific density of the product and the energy density used in the manufacturing process was determined [17]. In a previous study [18], a numerical tool based on the fluid dynamic model is presented to predict laser power and scan speed window to manufacture pore-free printed parts without lack of fusion and keyhole pores.

In this paper, an approximate method for determination of the process parameter window is presented based on the thermal limitations of the SLM processes.

2. THERMAL OPERATING WINDOW AND ITS PRELIMINARY DETERMINATION

If the energy of the laser beam indenting on the powder layer surface is sufficient, melting begins, and the solid–liquid interface is formed and propagates into the powder layer. The temperature and phase changes during the heat input are illustrated on Fig. 4. The thermal limitations of the SLM process are presented by points A and B.

The upper thermal limit relates to the possibility of occurrence of boiling, vaporising and injecting of the molten metal. Therefore, in this case, the isotherm (here, T_B) must be lower than the boiling point (Fig. 4).

The lower thermal limit guarantees that the powder layer is completely molten and, partially, the underlying layer is remelting to ensure proper bonding between the layers.

The SLM/SLS conditions that drive to these limits can be considered as critical and can be defined as *the thermal operating window*.

Comprehensive reviews of the thermal problems, modelling, computer simulations and experimental investigations of the SLM/SLS processes have been presented in numerous works [3–15].
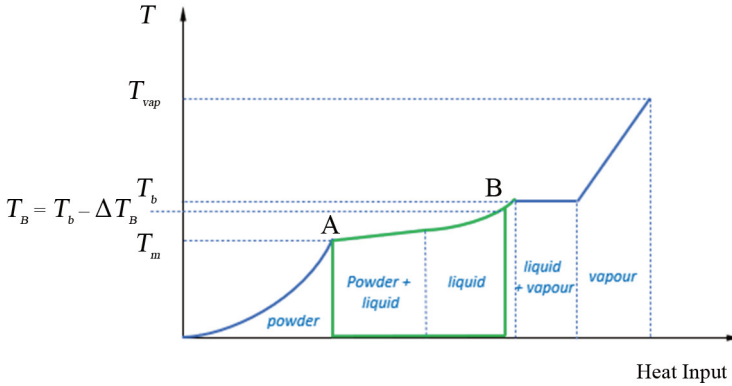
Figure 4. The diagram of phases changes during energy input into powder.
Point A with melting temperature T_m represents the lower thermal limit, and point B has temperature
$T_B = T_b - \Delta T_B$, where T_B is the upper thermal limit.

The determination of process windows from within a vast parameter space is a difficult task, especially for a large variety of feedstock powders used in SLM. The process window for each type of metal powder is typically determined through a sequential and time-consuming trial-and-error approach.

The paper presents the approximate approach for the determination of the critical conditions of the process and the operating window based on a simple thermodynamic model, in addition to its verification by means of computer simulation and experimental tests. The model has been developed with the basic idea of adequately representing the process within a simplified approach in order to reduce the computational time for practical use. For this reason, the model contains simplifications of the complex reality (surface tension effects, evaporation and thermo-flow dynamics are not simulated), aiming for a simplified simulation of heat transfer, leading to a reliable prediction of the operating window.

To find a relationship between the process parameters and the material's temperature, the simple model based on balance of the input energy and melt enthalpy of powder material is proposed in this section.

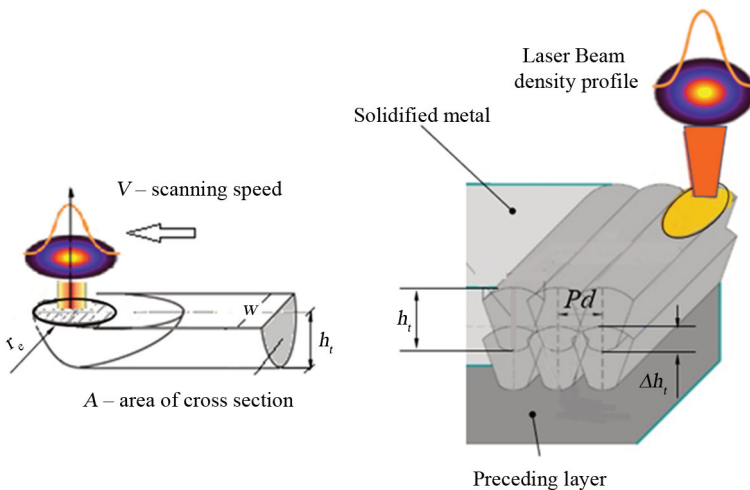Let us consider the melting process of a single track, as shown in Fig. 5.

Figure 5. The scheme of the single-track melting and multitrack structures.

In mathematical modelling, the following assumptions were made in order to approximately determine the thermal operating window of SLM:

- The powder phase is a quasi-homogenised continuum described by means of effective, i.e. spatially averaged, thermal and mechanical constant properties, without resolving the individual powder grains.
- The area of the cross-section of path A is expressed by the profile section coefficient k_p, which is defined as $k_p = A/wh_t$, where w is the track width.
- A quasi-steady-state SLM process is assumed, in which the average speed of the melting and solidification fronts is equal to the scanning speed. Therefore, the transient heat transfer, dynamics of molten metal, keyhole formation and dynamics of solidification are not considered.
- For the determination of the enthalpy in the process, the average equivalent heat capacity is used, which is defined as follows:

$$c_s = \frac{1}{T_m - T_0} \int_{T_0}^{T_m} c_p dT \qquad T_0 \leq T \leq T_m \tag{1}$$

$$c_l = \frac{1}{T_B - T_0} \int_{T_0}^{T_B} c_p dT \qquad T_0 \leq T \leq T_B$$

Let us make an energy balance for a unit of time; in this case, the mass of the powder melted by the laser beam is equal to:

$$M = \rho \, VA \tag{2}$$

After considering the cross-sectional profile of the path, we have:

$$M = \rho \, k_p w h_t V \tag{3}$$

Based on the mass conservation equation and taking into account the remelting of the underlying layer, we get the following:

$$h_t = (1 - \beta) h + \Delta h \tag{4}$$

where β is the porosity of powder layer, h is the powder layer thickness and Δh is the thickness of the remelted material of the underlying layer.

The example of a typical cross-section of a track is shown in Fig. 6.

The shape of the cross-sectional profile can be approximated by a parabolic curve (Fig. 7), where the coefficient profile $k_p = \frac{2}{3}$, or by an elliptical profile, where $k_p = \pi/4$.
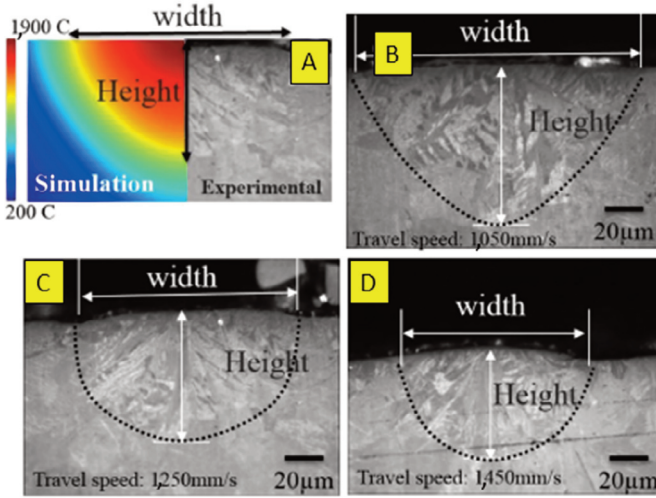
Figure 6. The cross-sections of the tracks (A) simulation vs experimental sample.
Track width at different laser travel speeds of (B) 1,050 mm/s, (C) 1,250 mm/s and (D) 1,450 mm/s
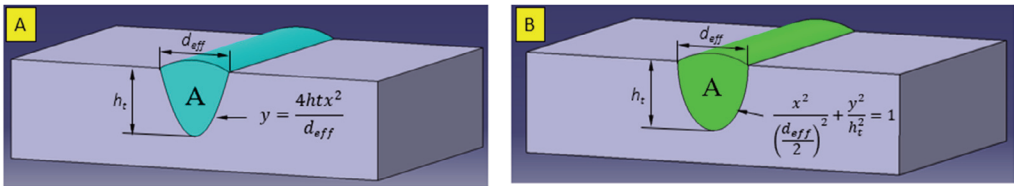(material: Ti-6Al; laser power: 175 W) (adopted from reference [8]).

Figure 7. Schematic approximation of the cross-section by parabolic profile (A) and elliptical profile (B).

Let us introduce the process efficiency coefficient being defined as $\eta = P_m/P$, where power P_m is the energy needed for melting over unit time and P is the laser beam power. The value of η depends on the laser energy transfer efficiency η_a and the melting efficiency η_m. The laser energy transfer efficiency is the ratio of energy that is being absorbed by the powder over the incident total laser energy, $\eta_a = P_a/P$. The second term is the melting efficiency η_m which describes the amount of energy that is used to create a molten pool in relation to the energy absorbed by the powder, i.e. $\eta_m = P_m/P_a$. Therefore, the process efficiency coefficient $\eta = (P_a/P)(P_m/P_a) = \eta_a \eta_m$.

The value of the energy transfer efficiency is determined experimentally, whereas the melting efficiency can be determined by computer simulation. A review of all the possible factors affecting the process efficiency is far beyond the scope of this paper.

Based on Figs 4 and 5 and the given assumptions, the energy balance for the lower and upper thermal limits is described as follows:

Point A – lower thermal limit (P_l):

$$\eta P_l dt = k_p \rho \, wVdt \left[(1-\beta)h + \Delta h\right]\left[c_s (T_m - T_0) + L_m\right] \tag{5}$$

Point B – upper thermal limit (P_u):

$$\eta P_u dt = k_p \rho wVdt \left[(1-\beta)h + \Delta h\right]\left[c_l (T_B - T_0) + L_m\right] \tag{6}$$

where $T_B = T_b - \Delta T_B$, the upper temperature limit for the thermal operating window (Fig. 3).

The temperature margin ΔT_B was introduced into the energy balance equation, Eq. (6), to prevent the molten material from boiling during the process, which may cause product defects.

The thickness of the remelted material Δh should be selected taking into account the structural integrity of the product.

The thermal limitations and processing window parameters of SLM are described by Eqs (5) and (6). The acceptable range of laser power from the point of view of product quality is as follows:

$$\frac{k_p \rho\, wV}{\eta}\Big[(1-\beta)h+\Delta h\Big]\Big[c_s\left(T_m-T_0\right)+L_m\Big] \leq P \leq \frac{k_p \rho\, wV}{\eta}\Big[(1-\beta)h+\Delta h\Big]\Big[c_l\left(T_B-T_0\right)+L_m\Big] \quad (7)$$

The relationship in Eq. (7) describes the initial prediction of the SLM thermal operating window on the plane {scanning speed V, laser beam power P}. It is a useful method for selection of the initial process conditions applying the software used in SLM practice, which is based on more accurate models. This approach significantly reduces the labour and time spent on the selection of SLM conditions.

3. COMPUTER SIMULATION OF THE SLM PROCESS AND EXPERIMENTAL INVESTIGATIONS

In order to determine the degree of compliance of the given approach with the real SLM process, a computer simulation was carried out using the COMSOL Multiphysics software developed by COMSOL, Inc. [19,20].

The software used in models more adequately describes and provides insight into the complex phenomena underlying the mechanisms of powder bed melting, transient thermo-fluid dynamics and solidification. It allows to take into account the influence of surface tension on molten metal conventions, as well as the evaporation and gas-cooling effects.

The general equation governing heat transfer during powder heating used in the COMSOL Multiphysics simulation is as follows:

$$\frac{\partial\left(\rho c_p T\right)}{\partial t}+\nabla\left(\rho c_p T \cdot \vec{v}\right)=\nabla\left(k_e \cdot \nabla T\right)+q \qquad (8)$$

where ρ is the density, ρ_{cp} is the specific heat at constant pressure, T is the temperature, v represents the velocity field, k_e is the effective thermal conductivity of the powder layer and q is the internal volume heat generation. Here, k_e is calculated in COMSOL as the combination of thermal conductivities of the metal and the protective atmosphere (N_2). For the needs of the mathematical model and computer simulation, an individual coefficient β (porosity) was determined for each layer's thickness, i.e. $h = 25$ μm, 30 μm and 35 μm. The porosity coefficient (β) of the powder was determined using CATIA V5 software developed by Dassault Systèmes based on the 3D model of the analysed powder bed.

The transport equations are applied to mass and momentum to describe velocity field of molten material.

Energy absorption depends on the heat source characteristicsThe laser beam power density distribution q_e for the SLM/SLS is assumed to be axisymmetric Gaussian.

$$q_e = \frac{2\eta_a P}{\pi r_e^2}\exp\left(-\frac{2r^2}{r_e^2}\right) \qquad (9)$$

where P is the laser power, r is the radial distance from the source's centre, r_e is the effective laser beam radius at which the energy density is reduced to $1/e^2$ at the centre of the laser spot.

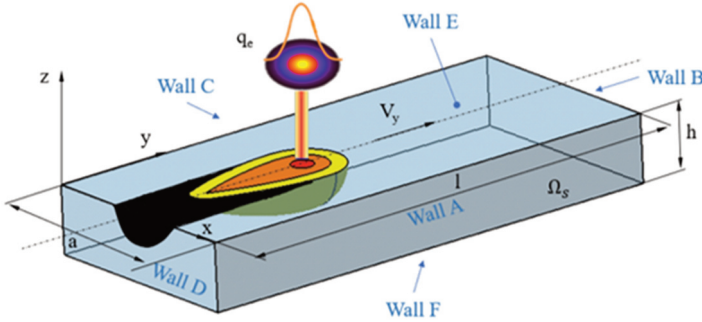The boundary conditions for Eq. (8) were assumed as shown in Fig. 8:

Figure 8. Scheme of heating of the powder layer. Model dimensions: a, h, l.

Figure 8 shows the simplified geometry as applied to the present boundary conditions for the mathematical model.

The boundary conditions for walls A, B, C, D, E and F were as follows:

$$k_e \frac{\partial T}{\partial n} = -\sigma_S \varepsilon \left(T^4 - T_a^4 \right) - \alpha_k \left(T - T_a \right) \tag{10}$$

where n is the direction normal to the considered wall, σ_S is the Stefan–Boltzmann constant, ε is the emissivity; α_k is the convective heat transfer coefficient and T_a is the ambient temperature.

- The phase change due to melting and solidification at the interface between the powder phase and the melt pool is described by the Stefan condition (Eq. 11); the indices e, s and l refer to the temperature gradients and thermal effective conductivity of powder and in the solid and liquid phases, respectively.

$$\text{melting } k_l \frac{\partial T}{\partial n} - k_e \frac{\partial T}{\partial n} = \rho L \frac{d n_{sl}}{dt} \tag{11}$$

$$\text{solidification } k_s \frac{\partial T}{\partial n} - k_l \frac{\partial T}{\partial n} = \rho L \frac{d n_{sl}}{dt}$$

where n_{sl} is the displacement of the moving solid–liquid interfaces along their normal direction n.

The 3D models of the powder bed were made in CATIA V5 software in the Part Design module.

For the purposes of the simulation, three variants of the bed layer models were created representing thicknesses h = 25 m, 30 m and 35 m with a grain diameter of 20 m.

The experiment was performed in the New Manufacturing Technologies Department at Lukasiewicz Research Network – Institute of Aviation.

The test samples were produced on the 3D Printer SISMA MySint 100. The machine has a laser with a spot diameter $2r_e$ = 55 m and a wavelength of 1,070 nm. During fabrication, the working chamber in the machine was filled with nitrogen gas to prevent oxidation of the fabricated specimens. The experiments were carried out using Mediloy S-Co powder (Co63.9Cr24.7W5.4Mo5.0Si) produced by BEGO GmbH & Co.

The physical properties of the powder were provided by manufacturer.

In the simulation, we assumed a change in the thermal conductivity coefficient of the powder material with temperature shown in Fig. 9.
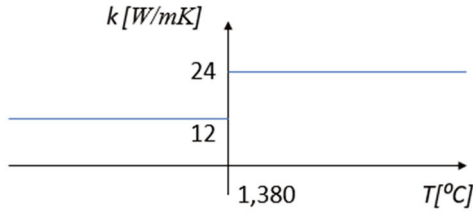

Figure 9. Thermal conductivity coefficient k_e for the powder material
for the solid and liquid phases.

The thermophysical properties and other parameters used in the simulation are given in Table 1.

Table 1. Thermophysical properties and other parameters used in simulation.

Physical properties of the powder		
Material density	ρ	8,600 kg/m^3
Specific heat capacity solid phase	c_s	390 J/kg·K
Specific heat capacity liquid phase	c_l	410 J/kg·K
Latent heat of melting	L_m	334 [kJ/kg]
Melting temperature	T_m	1,380 °C
Boiling temperature	T_b	2,930 °C
Upper temperature margin	ΔT_B	30 °C
Emissivity	ε	0.7
Process efficiency coefficient	η	0.27

The surface absorptivity of molten material strongly depends on its chemical composition and on the interaction with the surrounding atmosphere. For example, oxidation of the surface of the liquid material can cause a significant increase of absorptivity. However, in this study, we assume that the surface oxidation is negligible. This assumption is justified since the SLM process was performed under a protective atmosphere (nitrogen N$_2$).

The SLM process parameters used in the experiment and simulation are shown in Table 2.

Table 2. Process parameters.

Parameters	Lower limit	Upper limit	Unit
Laser beam power	70	170	W
Scanning speed	100	1,200	mm/s
Powder layer thickness	25	35	µm

The physics-controlled meshing for the 3D model of the powder bed body is shown in Fig. 10A. An example of the simulation results is presented in Fig. 10B.
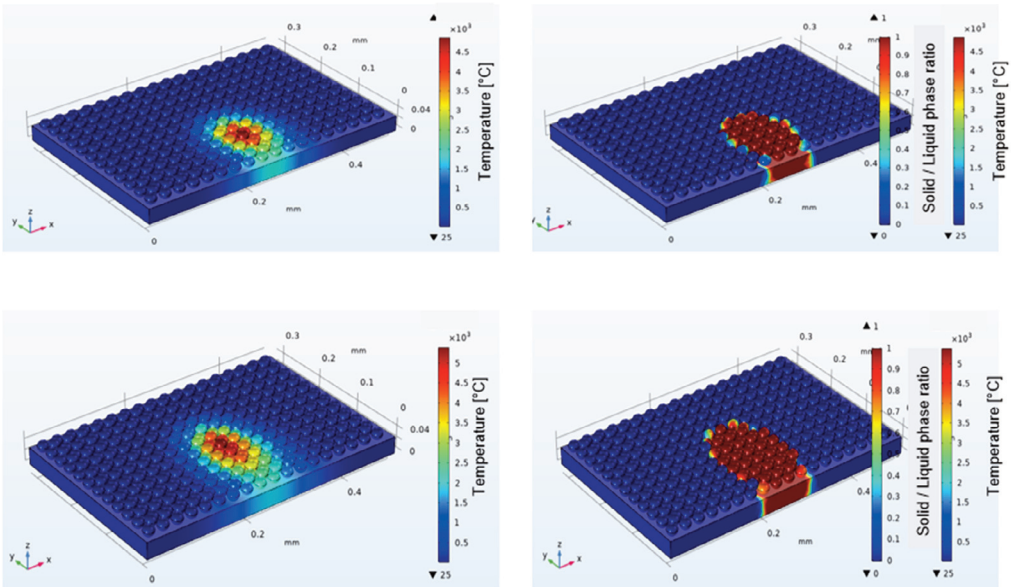
(A)
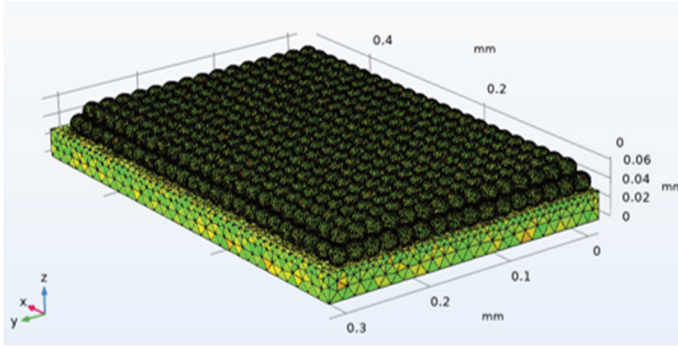
(B)

Figure 10. The model of the bed layer and the used mesh (A); simulation of heating and melting of powder with a laser beam (B).

The temperature distribution for the first layer is shown in Fig. 11, where the laser scanning direction is perpendicular to the drawing plane. The temperature isotherm curve is a series of quasi-ellipses. The position of the melting isotherm curve shows that the conditions are critical to the lower thermal limit due to the risk of incomplete melting of the powder layer.

Computer simulations of the unstable process using parameters outside the process window and a stable process using parameters inside the window were carried out. The plane of parameters {scan speed V, laser beam power P} are shown in Fig. 12.
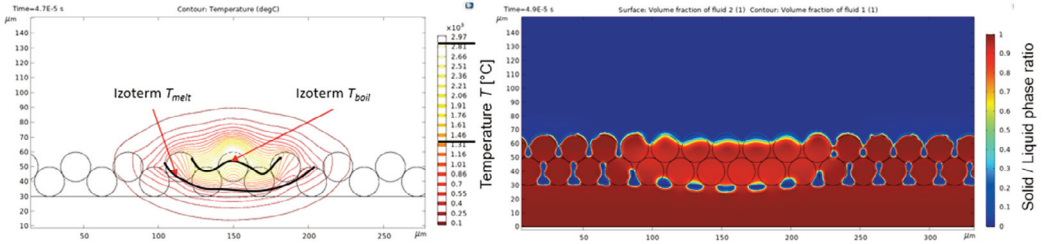
Figure 11. Plot of temperature distribution during heating P = 70 W, V = 1,200 mm/s. (cross-section perpendicular to the laser path; refer to Fig. 10).
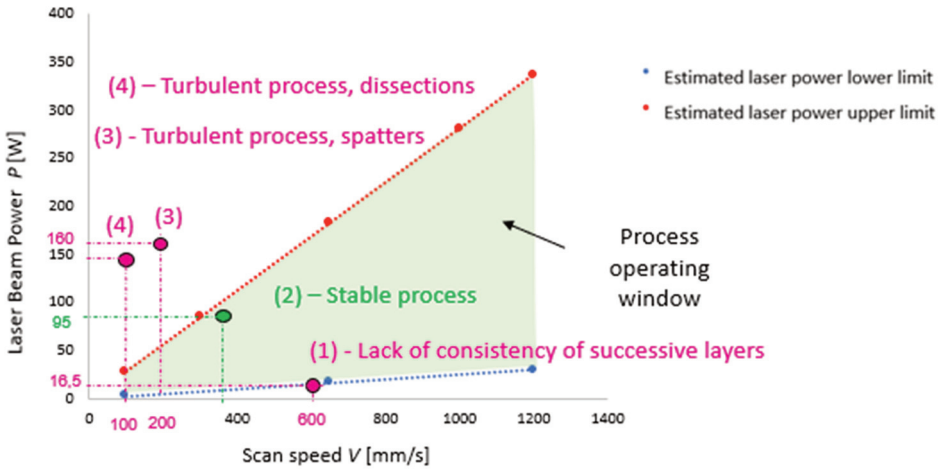

Figure 12. Plot of the operating window and results of simulation and experiments.
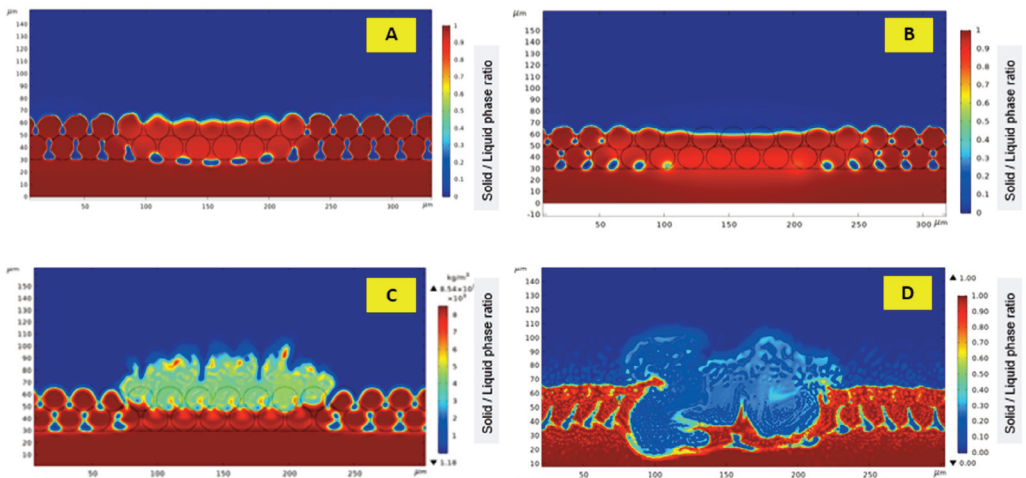

Figure 13. Simulation result of SLM at the following laser powers: (A) below lower thermal limit; (B) between lower and upper thermal limits; (C and D) exceeding the upper thermal limit. SLM, selective laser melting.

The result of simulation after exceeding the upper thermal limit is illustrated in Fig. 13, where the occurrence of ejection molten material, which leads to spatter, is shown. This result has been confirmed experimentally as shown in Fig. 14.
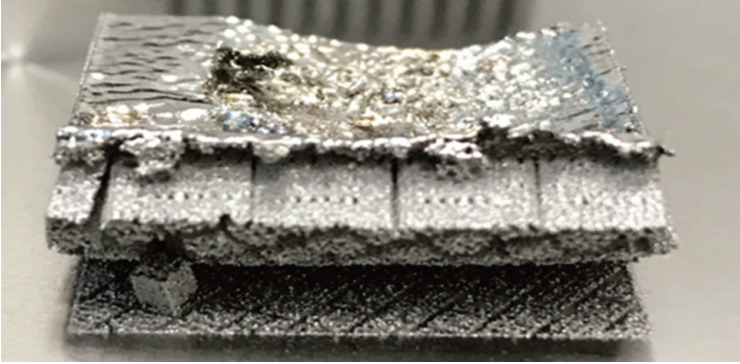

Figure 14. The result of the SLM when the process is carried out under conditions that exceed the upper thermal limit (sample dimensions: 21 mm × 21 mm × 10 mm).

The determined SLM operating window assuming a parabolic cross-sectional profile and the results of computer simulations and experimental tests are shown in Figs 12 and 15.
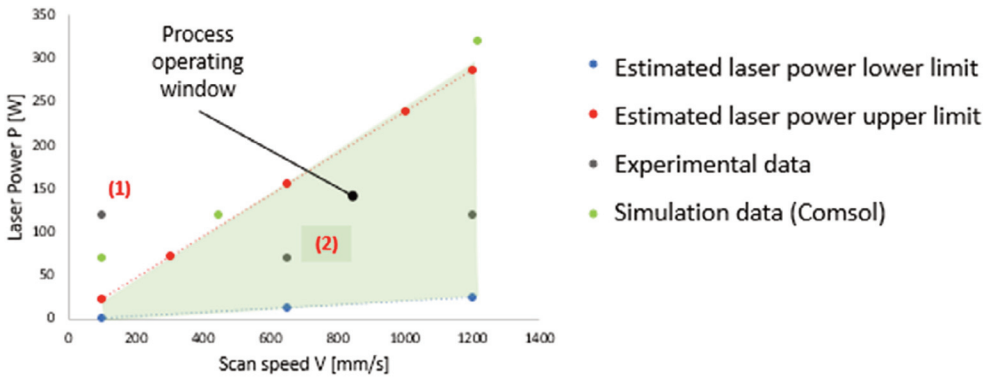

Figure 15. Plot of the operating window and results of simulation and experiments.

Figure 16 shows, as examples, the results of SLM processes carried out under conditions presented by points (1) and (2) in Fig. 15. In condition (1), outside the operating window, the quality of the sample is low, in particular, the (side) surface roughness parameters are Rz = 110 μm and Ra = 23 μm.

The SLM process carried out under condition (2), i.e. in the operating window, is characterised by products of a much higher quality, in particular, the surface roughness is many times lower, namely Rz = 23.6 μm and Ra = 6 μm.

Experimental studies have shown a fairly good agreement between the results of the approximate SLM model and the results of experiments and simulations. SLM processes performed with parameters from the approximate operating window were stable and showed acceptable product quality.
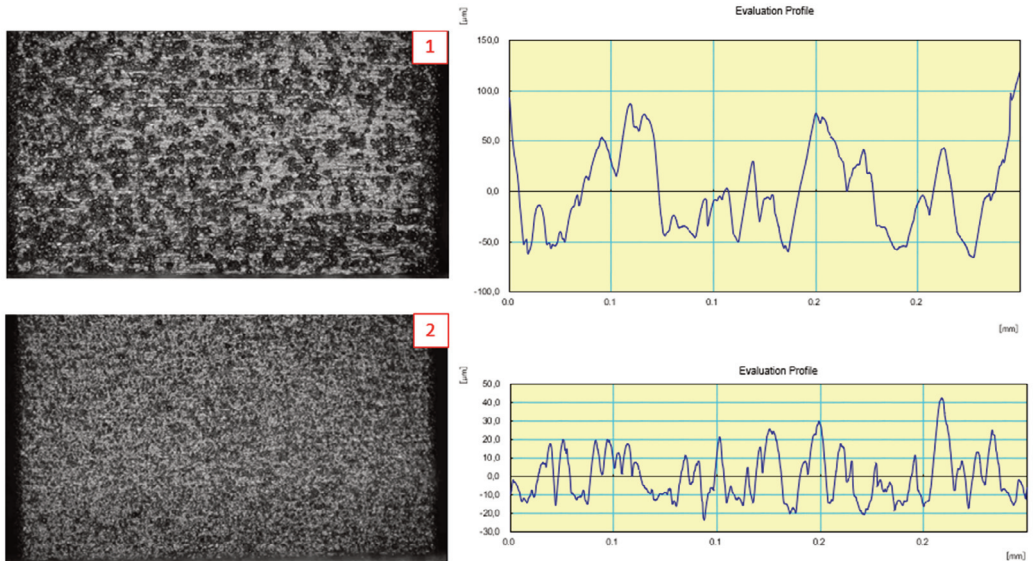
Figure 16. The surfaces obtained through experiments carried out in conditions represented
by points (1) and (2) in Fig. 15.

4. CONCLUSION

The paper presents an approximate determination of the operating window of the SLM process while maintaining thermal limitations. The determined thermal limits were confirmed by computer simulation and experiments. This allows to conclude about the usefulness of the approximate determination of the operating window for the preliminary selection of SLM conditions. In addition, it should be emphasised that all process parameters and material properties can be easily changed in the simulation code. This can be very helpful when trying to quickly determine a window of optimal process parameters for new materials.

REFERENCES

[1] The Next Generation and Future of GE | General Electric. Available at: https://www.ge.com/additive/sites/default/files/2020-08/GE9X%20Additive%20parts.pdf
[2] Kozak, J. and Zakrzewski, T. "Accuracy Problems of Additive Manufacturing using SLS/SLM Processes." *AIP Conference Proceedings*, 2018. DOI 10.1063/1.5056273.
[3] Meier, C., Penny, R.W., Zou, Y., Gibbs, J.S., and Hart, A.J. *Thermophysical Phenomena in Metal Additive Manufacturing by Selective Laser Melting: Fundamentals, Modeling, Simulation and Experimentation.* Mechanosynthesis Group, Department of Mechanical Engineering, Massachusetts Institute, Cambridge (2017).
[4] Zakrzewski, T., Kozak, J., Witt, M., and Dębowska-Wąsak, M. "Dimensional Analysis of the Effect of SLM Parameters on Surface Roughness and Material Density." *20st CIRP Conference on Electro Phisical and Chemical Machining XX, Book Series: Procedia CIRP*, Zürich (2021): pp. 115–120.
[5] Kozak, J., Zakrzewski, T., Witt, M., and Dębowska-Wąsak, M. "Selected Problems of Additive Manufacturing Using SLS/SLM Processes." *Transactions on Aerospace Research* Vol. 1 No. 262 (2021): pp. 24–44.
[6] DebRoy, T., Wei, H.L., and Zuback, J.S. "Additive Manufacturing of Metallic Components – Process, Structure and Properties." *Progress in Materials Science* Vol. 92 (2018): 112–224.

[7] Bayat, M., Dong, W., Thorborg, J., To, A.C., and Hattel, J.H. "A Review of Multi-Scale and Multi-Physics Simulations of Metal Additive Manufacturing Processes with Focus on Modelling Strategies." *Additive Manufacturing* Vol. 47 (2021): p. 102278.

[8] Dezfoli, Amir Reza Ansari, Hwang, Weng-Sing, Huang, Wei-Chin, and Tsai, Tsung-Wen. (2017). "Determination and Controlling of Grain Structure of Metals after Laser Incidence: Theoretical Approach." *Scientific Reports* Vol. 7 (2017): article: 41527.

[9] Kozak, J. *Mathematical Modelling of Advanced Manufacturing Processes*. Institute of Aviation Scientific Publications Division, Warsaw (2018).

[10] Zakrzewski, T. "Optimization SLS/SLM Process Conditions to Minimize Product Inaccuracy." PhD Dissertation. The Warsaw University of Technology. 2022. Available at: https://www.wip.pw.edu.pl/Media/RecenzjeKF/Streszczenie-pracy-mgr.-inz.-Tomasza-Zakrzewskiego

[11] Kruth, J.-P, Dadbakhsh, S., Vrancken, B., Kempen, K., Vleugels, J., Van Humbeeck, J., Srivatsan, T., & Sudarshan, T. (2016). Additive Manufacturing of Metals via Selective Laser Melting Process Aspects and Material Developments. In Additive Manufacturing: Innovations, Advances and Applications (pp. 69–99). CRC PRESS-TAYLOR & FRANCIS GROUP.

[12] Zeng, K.; Pal, D.; Stucker, B. A review of thermal analysis methods in laser sintering and selective laser melting. In Proceedings of the Solid Freeform Fabrication Symposium Austin, Austin, TX, USA, 6–8 August 2012; Vol. 60 (2012): 796–814.

[13] Kyogoku, H. and Ikeshojia, T. "A review of metal additive manufacturing technologies: Mechanism of defects formation and simulation of melting and solidification phenomena in laser powder bed fusion process", Mechanical Engineering Reviews, 2020, Vol. 7 (1): 19-00182

[14] Schoinochoritis, B., Chantzis, D., and Salonitis, K. "Simulation of Metallic Powder Bed Additive Manufacturing Processes with the Finite Element Method: A Critical Review." *Proceedings of the Institution of Mechanical Engineers, Part B: Journal of Engineering Manufacture*. 2017; 231(1): 96–117.

[15] Gong, K., Gu, H., Rafi, H., Starr, T., and Stucker, B. "Analysis of Defect Generation in Ti-6Al-4V Parts Made using Powder Bed Fusion Additive Manufacturing Processes." *Additive Manufacturing* Vol. 1 (2014): pp. 87–98.

[16] Engelhardt, A., Kahl, M., Richter, J., Krooß, P., Kroll, A., and Niendorf, T. "Investigation of Processing Windows in Additive Manufacturing of AlSi10Mg for Faster Production Utilizing Data-Driven Modeling." *Additive Manufacturing* Vol. 55 (2022): article: 102858.

[17] Ridolfi, M.R., Folgarait, P., and Di Schino, A. "Laser Operating Windows Prediction in Selective Laser-Melting Processing of Metallic Powders: Development and Validation of a Computational Fluid Dynamics-Based Model." *Materials* Vol. 13 (2020): article 1424.

[18] Ahn, I.H. "Determination of a Process Window with Consideration of Effective Layer Thickness in SLM Process." *The International Journal of Advanced Manufacturing Technology* Vol. 105 (2019): pp. 4181–4191.

[19] COMSOL Multiphysics® version 5.6. COMSOL AB, Stockholm, Sweden. Available at: www.comsol.com

[20] Simulation of Laser Powder-bed Fusion Additive Manufacturing Process Using the COMSOL Multiphysics® software. COMSOL - Software for Multiphysics Simulation. Available at: https://www.comsol.com/paper/simulation-of-laser-powder-bed-fusion-additive-manufacturing-process-using-the-c-65242

[21] Zhu, J-N., Borisov, E., Liang, X., Farber, E., Hermans, M.J.M., and Popovich, V.A. "Predictive Analytical Modelling and Experimental Validation of Processing Maps in Additive Manufacturing of Nitinol Alloys." *Additive Manufacturing* Vol. 38 (Feb. 2021): article 101802.